Measurement of plasma cell-free mitochondrial tumor DNA improves detection of glioblastoma in patient-derived orthotopic xenograft models

Mair, Richard; Mouliere, Florent; Smith, Christopher G.; Chandrananda, Dineika; Gale, Davina; Marass, Francesco; Tsui, Dana W. Y.; Massie, Charles E.; Wright, Alan J.; Watts, Colin; Rosenfeld, Nitzan; Brindle, Kevin M.

DOI:
10.1158/0008-5472.CAN-18-0074

Measurement of plasma cell-free mitochondrial tumor DNA improves detection of glioblastoma in patient-derived orthotopic xenograft models.

Richard Mair[1, 2, 3] *, Florent Mouliere[1, 3, 4] *, Christopher G. Smith[1, 3], Dineika Chandrananda[1, 3], Davina Gale[1, 3], Francesco Marass[1, 3], Dana W. Y. Tsui[1, 5], Charles E. Massie[1, 3], Alan J. Wright[1, 3], Colin Watts[6], Nitzan Rosenfeld[1, 3 #], Kevin M. Brindle[1, 3, 7 #].

* co-first author ; # co-senior author

1. Cancer Research UK Cambridge Institute, University of Cambridge, Cambridge, UK.
2. Division of Neurosurgery, Department of Clinical Neurosciences, University of Cambridge, Cambridge, UK.
3. Cancer Research UK Major Centre - Cambridge, Cancer Research UK Cambridge Institute, Cambridge, UK.
4. Amsterdam UMC, Vrije Universiteit Amsterdam, department of Pathology, Cancer Center Amsterdam, Amsterdam, The Netherlands.
5. Department of Pathology, Memorial Sloan Kettering Cancer Center, New York, NY, USA
6. Institute of Cancer and Genomic Sciences, University of Birmingham, Birmingham, UK.
7. Department of Biochemistry, University of Cambridge, Cambridge UK.

Corresponding authors:
Kevin Brindle, kmb1001@cam.ac.uk
Nitzan Rosenfeld, nitzan.rosenfeld@cruk.cam.ac.uk

Short title: Detection of circulating mitochondrial DNA in glioblastoma.

Abstract

The factors responsible for the low detection rate of cell-free tumor DNA (ctDNA) in the plasma of glioblastoma (GB) patients are currently unknown. In this study, we measured circulating nucleic acids in patient-derived orthotopically implanted xenograft (PDOX) models of GB (n=64) and show that tumor size and cell proliferation, but not the integrity of the blood-brain barrier or cell death, affect the release of ctDNA in treatment naïve GB PDOX. Analysis of fragment length profiles by shallow genome-wide sequencing (<0.2x coverage) of host (rat) and tumor (human) circulating DNA identified a peak at 145 bp in the human DNA fragments, indicating a difference in the origin or processing of the ctDNA. The concentration of ctDNA correlated with cell death only after treatment with Temozolomide and radiotherapy. Digital PCR detection of plasma tumor mitochondrial DNA (tmtDNA), an alternative to detection of nuclear ctDNA, improved plasma DNA detection rate (82% versus 24%) and allowed detection in cerebrospinal fluid (CSF) and urine.

Mitochondrial mutations are prevalent across all cancers and can be detected with high sensitivity, at low cost and without prior knowledge of tumor mutations via capture-panel sequencing. Coupled with the observation that mitochondrial copy number increases in glioma, these data suggest analyzing tmtDNA as a more sensitive method to detect and monitor tumor burden in cancer, specifically in GB where current methods have largely failed.

Keywords

Circulating DNA, mitochondrial DNA, Glioblastoma, Blood brain barrier, Patient-derived orthotopic xenograft.

Introduction

Release of DNA fragments from solid tumors, which can be collected in body fluids and used to identify and quantify tumor mutations, has created new possibilities for minimally invasive diagnosis and therapy monitoring (1,2). The concentration of cell-free tumor DNA (ctDNA) varies with cancer type, with some, such as glioblastoma (GB), showing extremely low plasma concentrations (3), which has hindered clinical translation.

Although ctDNA levels have been correlated with tumor burden (2,4) an understanding of the relationship between tumor biology and the release of ctDNA into the circulation is lacking, most notably for GB. Detection and measurement of ctDNA may be affected by both technical and biological factors (1,5). Recent work has related necrosis, tumor volume and proliferation to detection of ctDNA in patients with non-small cell lung cancer (2). However, no investigation of the effect of tumor biology on ctDNA release in GB has been performed.

Using a large cohort of patient derived orthotopically implanted xenografts (PDOX) (n=64) we investigated combined detection of circulating tumor mitochondrial DNA (tmtDNA) and ctDNA. Custom digital PCR (dPCR) was used to differentiate human mitochondrial DNA, originating from grafted tumor cells, from the host rat mitochondrial DNA. We demonstrated a higher frequency of detection and higher copy number for tmtDNA when compared with ctDNA in the plasma, cerebrospinal fluid (CSF) and urine of the xenografted rats. We used this improved yield to analyze the factors affecting tumor DNA release.

Release of ctDNA and tmtDNA in treatment naïve GB was associated with tumor volume and cell proliferation but not cell death. However, following

treatment with Temozolomide and radiotherapy (6), plasma tmtDNA was correlated with the levels of tumor cell death. Finally, bypassing blood brain barrier (BBB) integrity did not significantly affect the yield of ctDNA or tmtDNA.

Materials and Methods

Cell culture

Cells were obtained either locally or from the American Type Culture Collection (ATCC, Manassas, Virginia, US) and mycoplasma tested using RNA-capture ELISA. Cell line authentication was performed using STR genotyping contemporaneously with the experiments. U87 cells (ATCC) were cultured in Dulbecco's modified Eagle's medium, 2 mM L-glutamine (Gibco, UK) and 10% fetal bovine serum (Gibco, UK). Patient-derived cell lines were derived using protocols compliant with the UK Human Tissue Act 2004 (HTA licence ref. 12315), approved by the Local Regional Ethics Committee (LREC ref. 04/Q0108/60) and in accordance with the Declaration of Helsinki. GB tissue was minced and cells filtered (40 µm) (Falcon, UK) and washed with red blood cell lysis buffer. Live cells were seeded at 1.5 x 10^4 cm^2 and grown as monolayer cultures on extracellular matrix (ECM)-coated flasks (Engelbreth-Holm-Swarm murine sarcoma – 1:10 dilution, Sigma, UK) in Neurobasal A (Gibco, UK), 2 mM L-glutamine (Sigma, UK), 1% Streptomycin/Penicillin/Amphotericin B (Invitrogen, UK), 20 ng/mL hEGF (Sigma, UK), 20 ng/mL hFGF (R&D systems, UK), 2% B27 (Invitrogen, UK) and 1% N2 (Invitrogen, UK) at 37.5°C in 5% CO_2..

Orthotopic tumor model

Procedures were performed in compliance with project and personal licenses issued under the United Kingdom Animals (Scientific Procedures) Act, 1986, and approved by the local Animal Welfare and Ethical Review Body. Patient-derived cells, below passage 20, were re-suspended at 2 x 10^5 cells $µL^{-1}$ and 5 µL were implanted stereotactically (2 mm anterior and 3 mm lateral to the bregma (right-side)) in 6 week-old female rnu/rnu athymic nude rats (Charles River, Germany; Harlan, UK) (n=64).

Subcutaneous tumor model

Patient-derived cells (GB4) were re-suspended at 2.5 x 10^4 cells μL^{-1} and 200 µl injected subcutaneously into the right flank of 6 athymic nude rats.

Sample collection

Whole blood was taken via tail vein cannulation or peri-mortem via cardiac puncture and exsanguination. Coagulation was inhibited by adding 4.5 mmol/L EDTA to a maximum of 6 mL of blood. CSF was collected peri-mortem via cisterna magna puncture (7) and urine by direct bladder cannulation. Samples were centrifuged (4°C,1500 x g for 10 mins then 20,000 x g for 10 mins) before freezing (-80 °C).

DNA extraction

DNA from plasma (~1 mL), CSF (~100 µL), and urine (~100 µL) was extracted with the QIAamp Circulating Nucleic Acids kit (QIAGEN), elution volume 50 µL. Fragments of the *Xenopus Tropicalis* genome were spiked into the samples to estimate DNA extraction efficiency (Forward PCR primer - 5'-GTGATCATGGGATTTGTAGCTGTT - 3'; Reverse PCR primer – 5' AAACCAACCTGAAAACCATGGA - 3').

Western blot

Cell or tissue samples were lysed in RIPA buffer with 1% protease inhibitor (Thermo Fisher, Waltham, MA, US), run on BIS-TRIS gels (Thermo Fisher) transferred onto nitrocellulose membranes and incubated with nestin (Atlas, Stockholm, Sweden 1:100) and β-Actin (Abcam, 1:5000) antibodies in Li-COR-Odyssey blocking buffer (Li-COR Biotechnology, Lincoln, NE, US) overnight at 4°C. Primary antibodies were visualized using fluorescently-labeled anti-mouse or anti-rabbit Li-COR secondary antibodies and a LI-COR Odyssey CLx imaging system (LI-COR biotechnology, Lincoln, NE, US).

Chemoradiation

Rats were anesthetized with 1-2% isoflurane (Isoflo, Abbotts Laboratories Ltd., UK) and tumors irradiated via a lead collimator (15 Gy; Cs-137 irradiator

(IBL 637; CIS Bio International, France). Temozolomide (100 mg kg^{-1} was given by oral gavage 1 hour prior to radiotherapy.

Histopathology and Immunohistochemistry

Brains were placed in 10% formalin (Sigma-Aldrich, St Louis, US) for 24 hours, and then sectioned. Hematoxylin and eosin staining (H&E) (ST020 Multistainer – Leica Microsystems, Germany) was performed on 5 µm sections. TUNEL staining and immunohistochemistry (IHC) were performed on 10 µm sections. TUNEL staining used Leica's Polymer Kit (Leica Microsystems, Germany) and Promega's DeadEnd Colorimetric TUNEL System (Promega, US). IHC was performed using Leica's Polymer Refine Kit and human-specific antibodies: Ki67 – 1:200 dilution (M7240, Dako, Espoo, Finland), cleaved caspase 3 (CC3) – 1:200 dilution (9664, Cell Signalling Technology, Danvers, US), Glial Fibrillary Acid Protein (GFAP) – 1:10,000 dilution (Z0334, Dako, Espoo, Finland) and Carbonic Anhydrase 9 (CAIX) – 1:1000 dilution (AB1001, BioScience, Slovakia).

***In situ* hybridisation**

Pecam1 (CD31) mRNA was detected on 5 µm FFPE tissue sections with a probe for rat *Pecam1* (NM_031591.1, region 861 – 1766; RNAscope 2.5 LS red detection kit, 322150, Advanced Cell Diagnostics, USA) on a Leica Bond Rx (Leica Biosystems, Melbourne, Australia). Hybridization was detected using the Bond Polymer Refine Red detection kit (Leica Biosystems, DS9390) followed by counterstaining with haematoxylin. Probes targeting peptidylprolyl isomerase B (*PPIB)* (NM_022536.2, region 95 – 830) and *Dabp* (EF191515, region 414 – 86) were used as positive and negative controls, respectively.

Image analysis

Images, were annotated manually and analyzed using in-house algorithms (Aperio, Leica)

Digital PCR

Digital PCR was performed using Fluidigm 12.765 and 37k dPCR chips (Fluidigm, US). For targeting human nuclear DNA: 5 µl of TaqMan Gene Expression Master Mix, 0.5 µl of buffer, 0.5 µl of EVAGREEN (Biotium, Hayward, CA, US) and 1 µl of 10 µM forward primer (5'-TCACTCAAAGCCGCTCAACTAC-3') (Invitrogen, US) and 10 µM reverse primer (5'-TCTGCCTTCATTTCGTTATGTACC-3') (Invitrogen, US) were mixed with 3.5 µl of DNA. Primers for identifying human mitochondrial DNA were: forward 5'-ATACCCATGGCCAACCTCCT-3', reverse 5'-GGGCCTTTGCGTAGTTGTAT-3'. Primers for identifying rat DNA were: forward 5'-CCACCCCCTGGGCTCTGTT-3', reverse 5'-CCCGGATCCCCTGCGTGAGA-3'. Assays for human DNA (ctDNA) and rat DNA (non-tumor cell-free DNA (nt cfDNA)) targeted the human (*RPP30* gene) and rat (*RPP30* gene) sequences, respectively, in copy number neutral regions where there was no homology with the reciprocal rat and human genomes.

Shallow whole genome sequencing

Libraries were prepared using a NEB ultra v2 kit (New England Biolabs, Ipswich, US). Ten ng of tumor issue DNA was sheared to 150 – 200 bp with an ultra-sonicator (Covaris, Woburn, US). For plasma and CSF samples, we selected rats with concentrations of ctDNA greater than 1000 copies/mL, as determined by dPCR. Libraries were pooled in equimolar amounts and sequenced on a HiSeq 2500 (Illumina, San Diego, US) generating 125 bp paired-end reads. Reads were aligned and localization of somatic copy number aberrations was estimated by QDNAseq (8).

Magnetic Resonance Imaging

We used a 7T spectrometer (Agilent, Palo Alto, US) and a 72 mm inner-diameter ^{1}H quadrature birdcage coil (Rapid Biomedical GMBH, Rimpar, Germany). Animals were anesthetized with 1-2% isoflurane in O_2. Axial T_2-weighted images were acquired using a fast spin-echo sequence (TR, 1.5 s; TE, 40 ms; 256 x 256 data points over a 40 x 40 mm field-of-view (FOV), 4-8 averages) from fifteen 2 mm thick slices. A T_1-weighted spoiled gradient echo sequence (27° flip angle, TR 43 ms, TE 4.6 ms, FOV 40 mm x 40 mm, 256 x

128 data points) was used to acquire images before and 30, 60 and 90 s after injection of contrast agent (100 µmol/kg Dotarem; Guebert). Five axial slices, 1.5 mm thick and with a 0.3 mm gap between them were acquired. Images were transferred to MATLAB (The Mathworks, Natick, USA) and difference maps calculated, on a voxel-by-voxel basis, as the post contrast image minus the pre-contrast image divided by the pre-contrast image.

Disruption of the blood brain barrier

Mannitol (2-2.5 mL of a 25% solution in 0.9% saline) was administered via a tail vein cannula. Rats immediately underwent diuresis, evident from urinary incontinence under anesthesia.

Demonstration of blood-brain barrier opening using dynamic contrast-enhanced magnetic resonance imaging

Images were acquired using the 72 mm diameter ^{1}H transmit coil and a 2-channel rat-head ^{1}H receiver coil placed over the brain. A fast spin-echo sequence (TR 2 s, TE 48 ms, FOV 4 cm x 4 cm, 2 mm thick slice, 256 x 256 data points) was used to acquire 4 axial brain slices from the same region where tumors were implanted in the other animals. Baseline T_1 measurements used an inversion recovery-spoiled gradient echo sequence (adiabatic inversion pulse, 8 inversion times between 0.05-10 s, scan repeat time 12 s, TR 2.08 ms, TE 0.92 ms, flip angle 10°, 4 x 1.8 mm thick slices with a 0.2 mm gap between slices). Dynamic contrast enhanced (DCE) images were acquired using a gradient echo sequence (TR 25 ms, TE 2.85 ms, flip angle 30°). A series of 100 images (2 averages, 6.4 s per set of 4 images) were acquired. Dotarem (0.2 mmol/kg; Gadoteric acid, Guerbet, France) was injected via a tail vein after the 10th time point image. Mannitol was administered immediately prior to the start of DCE image acquisition. Signals from the DCE time course were converted, on a pixel-by-pixel basis, to a contrast-agent concentration by assuming an R_1 relaxivity for Dotarem of 3.1 $s^{-1}mM^{-1}$ (9). An elliptical region of interest was drawn in each of the four slices, covering the thalamus to the pre-frontal cortex and an average DCE profile was calculated (10) using the same population-derived double-exponential arterial-input-function for each data-set (11). The calculated extravascular

and extracellular spaces per unit volume of tissue (Ve) accessible to the contrast agent were used as an indicator of blood brain barrier permeability.

Statistics

Statistics were performed using GraphPad Prism (GraphPad Software Inc, California, US) and R (www.r-project.org). Principal Component Analysis (PCA) was performed with R using the *factoextra* package.

Results

tmtDNA is a more sensitive marker of systemic tumor nucleic acids than ctDNA and is detected in multiple body fluids.

There are 10^2 - 10^5 copies of the 16.5 kb mitochondrial genome per human cancer cell (12) and therefore tmtDNA released into the circulation may be a more sensitive marker of tumor burden than ctDNA (13). We used dPCR to investigate the levels of tmtDNA and ctDNA in different rat PDOX models of GB, which were derived from tumor material taken from different GB patients. The selected dPCR assays were chosen from among 9 dPCR assays. Specificity for human (in the PDOX models this represents tumor DNA) and rat (host) DNA was determined using plasma DNA from 4 healthy human individuals and 4 non-grafted rat controls (**Fig. 1a**). Human nuclear DNA levels averaged 7469 copies/mL and human mitochondrial DNA averaged 38091 copies/mL in the human plasma samples, where copies/mL represents the number of amplifiable copies in the dPCR reaction. Rat nuclear DNA was not detected in the human plasma and human nuclear DNA was not detected in rat plasma, despite a high concentration of rat nuclear DNA (15610 copies/mL). Only very low amounts of human mitochondrial DNA (mean 3 copies/mL, <0.02%) were detected in rat plasma.

The sensitivity of our selected ctDNA and tmtDNA assays were determined with a duplicate dilution series of human DNA in rat plasma DNA. The

tmtDNA assay could detect the presence of human DNA at dilution levels 100x greater than the ctDNA assay, and could detect the presence of human mitochondrial DNA even when human nuclear DNA could no longer be detected (**Fig. 1b**).

Six representative PDOX models of GB (GB1, 8 rats; GB2, 8 rats; GB3, 3 rats; GB4, 36 rats; GB5, 6 rats and GB6, 3 rats) were studied. In total 64 animals were analyzed using the dPCR assay. As shown previously (14) these models showed much slower growth rates than tumors arising from implantation of a GB cell line (U87) (**Supplementary Fig. S1a** and **Supplementary Table 1**) and much higher levels of expression of glial fibrillary acidic protein *in vivo* (15) (**Supplementary Fig. S1b**) and nestin, a neural stem cell marker, *in vitro* (16), which were largely absent from U87 tumors and cells respectively (**Supplementary Fig. S1c**). All showed histological features of GB (**Supplementary Fig. S1d**).

Plasma ctDNA was detected in all but one cohort (GB1), with a detection rate of 24% across all animals (15/64) and at an average concentration of 27 tumor haploid genome equivalents per mL (copies/mL of the targeted human sequence) (**Fig. 2a, b**). Plasma tmtDNA was identified in all the PDOX cohorts with a detection rate of 82% (52/64) and an average concentration of 5081 copies/mL (~190-fold higher than the mean value for ctDNA) (**Fig. 2a, b**). Non-tumor (rat host) cell-free nuclear DNA was detected in all the animals at considerably higher concentrations than ctDNA (t-test, $p<0.001$) with a mean concentration of 6989 copies/mL (**Fig. 2a, b**). Variable detection rates were observed between the different PDOX models, with tmtDNA detected in 66% of some models (GB1; n = 8) and 100% in others (GB5; n = 6) (**Supplementary Fig. S2a**). ctDNA and tmtDNA were not detected in plasma from non-grafted animals (n=4), (**Supplementary Fig. S2b**).

ctDNA has been detected at low concentrations in urine from patients with non-brain tumors (17). Urine samples from 11 tumor-bearing animals (10 GB4 and 1 GB5) had undetectable levels of ctDNA. However, tmtDNA was identified in 60% of samples with a median concentration of 606 copies/mL

(**Figure 2c, d**). The CSF presents another possible source of cell-free tumor DNA. We collected an average of 97 µL of CSF (7) from 12 PDOXs (10 GB4, 1 GB1 and 1GB2). ctDNA was detected in 4 out of 12 samples (median concentration of 222 copies/mL) and tmtDNA was detected in all samples (median concentration of 760 copies/mL) (**Fig. 2c, d**). Rat host cell-free nuclear DNA was detected in all samples with a median concentration of 215 copies/mL.

ctDNA and tmtDNA levels correlate with tumor size and cell proliferation in treatment naïve PDOXs

We performed principal component analysis (PCA) on 8 tumor-related variables in treatment naïve GB4 models (n=36). The first component included plasma ctDNA and tmtDNA concentrations, tumor volume and Ki67 staining, a marker of cell proliferation, and the second component the plasma concentration of host non-tumor cell-free nuclear DNA (nt cfDNA), staining for TUNEL and cleaved caspase 3 (CC3), which are cell death markers, and carbonic anhydrase 9 (CAIX), a marker of hypoxia (**Fig. 3**). Correlations (Pearson analysis) were observed between tmtDNA and ctDNA (R^2=0.83, p<0.001), tumor-derived DNA and tumor volume (tmtDNA R^2=0.86, p<0.001; ctDNA R^2=0.83, p<0.001) and tmtDNA and ctDNA and the number of proliferating cells (Ki67 positive cells) (tmtDNA R^2=0.54, p<0.001, ctDNA R^2=0.54, p<0.001). We also observed a correlation between nt cfDNA and cell death (TUNEL R^2=0.62, p<0.001 and CC3 R^2=0.47, p<0.01). Tumor microvessel density was not significantly different between the different PDOX models (p=0.27) (**Supplementary Fig. S3**).

ctDNA and tmtDNA levels correlate with cell death following treatment with Temozolomide and radiotherapy

In GB4 (n=36) tmtDNA and ctDNA were highly correlated with tumor volume (R^2=0.8; p=<0.0001) (**Fig. 4a**), suggesting that tmtDNA, like ctDNA, could be used to track tumor burden and monitor treatment response.

We analyzed plasma from GB4 PDOX models 72 hours after treatment with Temozolomide plus radiotherapy (15 Gy, n=7). ctDNA detection frequency and concentration increased (from 40%, 7 copies/mL to 75%, 54 copies/mL, p=0.051), (**Fig. 4b**). tmtDNA concentration also increased (from a median 121 copies/mL to 256 copies/mL, p=0.094), (**Fig. 4b**) but detection frequency remained unchanged (6/7 cases). These increases in ctDNA and tmtDNA concentrations were associated with an increase in tumor cell death, as assessed by TUNEL (p=0.039) (**Fig. 4c**) and CC3 staining (p=0.037) of tumor sections (n=7) (**Fig. 4d**), with a correlation being observed between ctDNA and CC3 staining (R^2=0.58, p=0.074, Pearson analysis), which is a marker of early apoptosis (18).

These data indicate that in treatment naïve models, tumor DNA release was related to tumor burden and cell proliferation, whereas following treatment, tumor DNA was released primarily through tumor cell death.

Genome-wide sequencing showed a different fragmentation pattern for ctDNA and host DNA in treatment naïve PDOXs

We used genome-wide sequencing at low coverage (<0.2x) to determine copy-number profiles of host rat and human (tumor) nuclear genomes in plasma, CSF and tumor tissue. Paired-end sequencing reads were aligned to rat (RGSC 6.0 / rn6) and human (hg19) genomes, and assigned to the appropriate species (**Fig. 5a**). Similar copy number profiles were found in tumor DNA from the different fluid compartments and from tumor tissue (**Fig. 5b**), even though the plasma compartment exhibited a lower tumor DNA fraction, relative to host DNA, when compared with tumor tissue and CSF. We also determined the size distribution of human (tumor) and rat (host) circulating nuclear DNA fragments (**Fig. 5c-e**) in the plasma of animals grafted with GB6 (**Fig. 5c**) and with GB4 (**Fig. 5d**). We also determined, for one animal implanted with GB4, the size distribution of the DNA fragments from CSF (**Fig. 5e**). The fragment size distribution in plasma and CSF showed a peak at 133-145 bp for human (tumor) DNA, and a different fragmentation pattern for host rat DNA, with a peak at 167 bp (**Fig. 5c-d**). Mitochondrial DNA

showed a peak below 100 bp for both human (tumor) and rat circulating mitochondrial DNA (**Fig. 5f**), in agreement with previous work (19).

The blood-brain barrier has a limited effect on plasma ctDNA and tmtDNA concentrations

Despite extensive disruption of the BBB during gliomagenesis (20), the low levels of ctDNA observed in the plasma of GB patients and the apparent enrichment of tumor DNA in the CSF have been attributed to the impermeability of the BBB (3). This was supported by sequencing, where tumor mutations in DNA from the CSF of GB patients were detected more frequently than in plasma and at higher mutant allele fractions (21,22). However, the absolute concentrations of tumor and non-tumor DNA in CSF and in plasma of GB patients have not been reported previously. The data shown in Figure 2 show that the higher detection rate of tumor DNA in CSF is due to a higher concentration of ctDNA relative to host nt cfDNA in CSF (222 copies/mL ctDNA versus 215 copies/mL nt cfDNA) when compared to plasma (27 copies/mL ctDNA versus 6989 copies/mL nt cfDNA). We investigated this further by using dPCR to quantify the concentrations of tmtDNA in plasma and CSF samples collected from 12 of the tumor models (GB1 (n=1), GB2 (n=1), GB4 (n=10)). tmtDNA concentration was higher in CSF as compared to plasma in each of the tumor models (**Fig. 6a**), with a median of 476 copies/mL in CSF and 93 copies/mL in plasma. However, CSF volume in the rat is ~90 µL and the plasma volume ~6 mL (23) and therefore the total amount of tmtDNA in the plasma (558 copies) is ~13 times higher than in the CSF (43 copies), showing therefore that the BBB does not prevent significant amounts of tumor DNA, at least tmtDNA, from reaching the circulation. Whereas the concentration of tumor-derived cell-free DNA was 5~8-times higher in CSF compared to plasma, the concentration of nt cfDNA was nearly 25 times higher in plasma compared to CSF. Therefore, lower detection rates of tumor-derived DNA in plasma are due, at least in part, to the presence of higher levels of background host DNA in plasma.

To investigate more directly the effect of the BBB on plasma tmtDNA and ctDNA concentrations, we used subcutaneous implantation of GB4 cells to generate a GB model that was outside the BBB. We also disrupted the BBB by intravenous administration of mannitol (24). Following mannitol injection, sixty minutes were allowed for ctDNA to escape into the circulation before plasma collection. If the BBB blocks release of tumor DNA into the circulation, then sixty minutes after mannitol injection there should be an increase in tumor DNA levels in the circulation, given that maximal BBB opening occurs 5 min following mannitol infusion (24) and the circulating DNA half-life is 16 min (25). Gadolinium-based contrast agents do not cross the intact BBB and are used commonly for MR imaging of BBB breakdown in GB (26). We confirmed in 3 control rats that mannitol infusion caused BBB disruption using dynamic contrast-enhanced MRI measurements. Within 10 minutes of mannitol administration there was an increase in the fraction of tissue accessible to the contrast agent ($p<0.02$) and in the contrast agent concentration (untreated; 6.3±4.0 μM (SD), post mannitol; 14.8±1.8 μM (SD), $p<0.025$ (one sided Welch's t-test) (**Supplementary Fig. S4a,b**). There were no significant differences in the concentrations of ctDNA or tmtDNA between the three groups, after normalization to tumor volume, which was determined using T_2-weighted MRI (orthotopic model) and caliper measurements (subcutaneous model) (one-way ANOVA $p=0.57$ and individual t-tests; n=16) (**Fig. 6b**). Moreover, the tumor volume-corrected concentrations of ctDNA detected in animals with subcutaneous GB tumors were much lower than those reported for animals implanted subcutaneously with other tumor types (27, 28). Analysis of CD31 expression (an endothelial cell marker) showed increased microvessel density in subcutaneous versus orthotopic tumors ($p=0.0173$) (**Fig. 6c**), however there was no significant difference in the ctDNA or tmtDNA levels (**Fig. 6b**), suggesting that release from the subcutaneous tumors was not affected by vascular density. Comparison of ctDNA and tmtDNA concentrations in contrast agent enhancing (GB4, GB3) and non-enhancing (GB1, GB5) tumors showed no differences in ctDNA ($p=0.65$) or tmtDNA concentrations ($p=0.49$) between these groups (**Fig. 6d**).

Discussion

Detection of ctDNA in GB patients is challenging because of low plasma concentrations (3). Sampling of cerebrospinal fluid (CSF) has been proposed as a method for detecting ctDNA in GB (21,22,29), however, lumbar puncture is contraindicated in patients with intracerebral space occupying lesions and thus routine use of this technique is not clinically feasible (30,31). Nevertheless, the requirement for minimally invasive techniques that avoid repeated biopsies in GB patients remains due to current inadequacies in identifying treatment response/escape (32) and the evolving nature of the disease during treatment (33-35). We therefore pursued methods to improve detection of circulating tumor-derived nucleic acids through the use of PDOX models of GB and used these methods to identify factors affecting DNA release.

Digital PCR was used to estimate plasma tmtDNA and ctDNA concentrations in a large number of PDOX models of GB. The detection rate for tmtDNA was 82% in plasma samples (n=64), at an average concentration of 5081 copies/mL, versus a detection rate for ctDNA of 24%, at an average concentration of 27 copies/mL. Host cell-free nuclear DNA concentrations have a broad range and the values we report are within the range reported previously for animal models (27, 28). tmtDNA was also detected in 60% of urine samples in which ctDNA was undetectable. Because tmtDNA is highly fragmented in plasma (**Fig. 5f**), *in vitro* or *in silico* size selection of fragments below 100 bp could be used to sieve tmtDNA from nuclear ctDNA, enriching the sample for tmtDNA and further enhancing the sensitivity of detection (36). The potential for tmtDNA to be used to detect smaller tumors, either at diagnosis or at recurrence would be important clinically.

Using both ctDNA and tmtDNA we investigated the factors influencing release of tumor-derived nucleic acids into the circulation. The levels of both were

correlated with tumor size, in agreement with previous pre-clinical (27,28) and clinical (3,25) studies. Previous analyses of cell-free DNA fragment sizes in plasma showed these to be mostly distributed around 167 bp, and multiples thereof, characteristic of caspase-dependant cleavage and suggesting that the majority of cell-free DNA originates from apoptosis (37,38). In cancer patients, a shortening of cfDNA was observed (39,40), which could reflect modifications in chromatin organization (41,42). Recent work on fetal cell-free DNA suggested that methylation-related chromatin re-organization can result in shortening of fragment length (38,43). The first comprehensive analysis of the relationship between tumor physiology and ctDNA in patients indicated that cell proliferation and tumor volume are more strongly correlated with ctDNA concentration than cell death (2). Here we have shown, in treatment naïve PDOX models, that there is a correlation between non-tumour (host) cell-free DNA levels and cell death. Fragmentation analysis showed a distribution centered around 167 bp, consistent with release from apoptotic host cells. We observed a correlation between ctDNA levels and tumour volume, and to a lesser extent with cell proliferation, but not with cell death, as was observed previously (2). Analysis of ctDNA fragment sizes revealed a shift towards shorter fragment sizes, with a distribution centred around 145 bp, corresponding to the core nucleosome. These findings suggest that size selection could potentially be used to improve the yield of ctDNA fragments (36).

The concentrations of plasma ctDNA and tmtDNA were increased following Temozolomide and radiotherapy treatment and, in this instance, were related to an increase in tumor cell death. However, CC3 and TUNEL staining only inform upon a proportion of dying cells and not those affected by mitotic catastrophe or senescence for example. In these treated animals there was no longer any correlation between plasma levels of ctDNA and tmtDNA and cell proliferation. Therefore, it appears that release of tumor DNA pre and post treatment occurs via different processes. DNA release via cell death post treatment, may be explained by the requirement for tumor cells to be in close proximity to viable blood vessels, which provide the oxygen necessary for radiotherapy-induced tumor cell kill (44). Thus, when these cells die, they do

so in a vessel rich microenvironment, and are distinct from dying tumor cells in treatment naïve GB, where cell death may occur predominantly in cells with a poor blood supply.

The BBB has been proposed as the main reason for reduced ctDNA detection in GB (21). Our experiments, in which we circumvented the BBB via heterotopic tumor engraftment or opened the BBB using mannitol, suggest that the effect of the BBB on release of tumor-derived DNA into the plasma may be less significant than previously thought. Recent studies have shown higher relative levels of mutant DNA in CSF compared to plasma of GB patients (21,22), which has been interpreted as being due to enrichment of tumor DNA in the CSF. Using dPCR to measure absolute concentrations of tumor and host DNA we found that higher relative levels of tumor DNA in CSF resulted primarily from lower concentrations of non-tumor host DNA together with more modest increases in the quantity of tumor-derived DNA.

Whilst we used single-copy human mitochondrial sequences to identify tmtDNA in the PDOX models, this strategy is not directly applicable to a human patient. However, mitochondrial mutations are present in the majority of cancers, with frequencies depending upon the tumor of origin, and mutational ‘hotspot’ regions have been identified (45), suggesting that mutated mitochondrial sequences could be used to detect tmtDNA in the clinic (12). Whole genome sequencing (WGS) has enabled detection of mitochondrial DNA variant-allele fractions down to 1% (46), moreover studies have shown that certain tumors positively select for non-synonymous mitochondrial DNA mutations (47). Although WGS is expensive, the small size of the mitochondrial genome means that targeted, and/or capture-sequencing based methods could provide a more affordable alternative and may enable improved sequencing depth (48). Genome-wide or targeted sequencing of the tumor tissue DNA obtained at surgery may also permit strategies whereby dPCR probes or focused sequencing assays may be employed to track tmtDNA mutations in plasma.

Several cancers have higher mitochondrial copy numbers, thus further increasing the probability of detecting tmtDNA (49). Detection of ctDNA in IDH1-mutant glioma, for example, has demonstrated limited clinical efficacy (3), however the high tmtDNA copy number in these tumors may make circulating tmtDNA analysis achievable (49). Recent studies have identified certain cancers with functional tmtDNA mutations that affect metabolism (46). This could be used to target metabolic therapies to tumors with known metabolic weaknesses (46). tmtDNA mutations have also been described which confer specific chemoresistant properties (50). Thus their monitoring via serial liquid biopsy may enable therapy modulation, as has been demonstrated with the use of ctDNA (4).

In conclusion, release of tmtDNA and ctDNA is correlated with tumor volume and tumor cell proliferation in treatment naïve tumors and with tumor cell death following treatment. The blood brain barrier appears to play only a minor role in preventing release of glioma-derived ctDNA into plasma. Analysis of circulating tmtDNA can improve the sensitivity of detection of tumor DNA in multiple body fluids and may make plasma liquid biopsy possible for patients with gliomas, where detection rates for ctDNA have so far been very low.

Acknowledgements

The authors would like to acknowledge Prof. Richard J. Gilbertson and Dr. Irena Hudecova for fruitful discussions. We wish to thank for their help and support the Cancer Research UK Cambridge Institute core facilities, in particular the biological resource unit, genomics, histopathology and pre-clinical imaging sections. We wish also to thank the Cambridge Molecular Diagnostic Laboratory, and in particular Dr. Mikel Velganon. We would like to thank also Mr Stephen Price, Dr De-en Hu, Ms Leigh-Anne McDuffus, Ms Jodi Miller, Ms Bev Wilson, Ms Julia Jones, Mr Mike Mitchell, Ms Lisa Young and Ms Gemma Bullen.

N. Rosenfeld and K. Brindle are supported by the University of Cambridge, Cancer Research UK (grant numbers A11906, A20240, 17242, 16465) and Hutchison Whampoa Limited. N. Rosenfeld has received funding from the

European Research Council under the European Union's Seventh Framework Programme (FP/2007-2013) / ERC Grant Agreement n. 337905. C. Watts is supported by The Brain Tumour Charity grant 10/136.

Competing interests

Nitzan Rosenfeld and Davina Gale are co-founders, shareholders and officers/consultants of Inivata Ltd, a cancer genomics company that commercialises circulating DNA analysis. Nitzan Rosenfeld has research funding from Astra Zeneca. Christopher G. Smith has consulted for Inivata Ltd. Francesco Marass has patents and shares in Inivata Ltd. Dana Tsui has honoraria with Astra Zeneca and the National Taiwan University and has consulted for Inivata. Inivata had no role in the conception, design, data collection and analysis of the study. Other co-authors have no conflict of interests.

References

1. Wan JCM, Massie C, Garcia-Corbacho J, et al. Liquid biopsies come of age: towards implementation of circulating tumour DNA. Nature Rev Cancer. 2017;17:223–38.

2. Abbosh C, Birkbak NJ, Wilson GA, et al. Phylogenetic ctDNA analysis depicts early-stage lung cancer evolution. Nature. 2017;545:446–51.

3. Bettegowda C, Sausen M, Leary RJ, et al. Detection of circulating tumor DNA in early- and late-stage human malignancies. Sci Transl Med. 2014;6:224ra24.

4. Dawson S-J, Tsui DWY, Murtaza M, et al. Analysis of Circulating Tumor DNA to Monitor Metastatic Breast Cancer. N Engl J Med. 2013;368:1199–209.

5. Wang J, Bettegowda C. Applications of DNA-Based Liquid Biopsy for Central Nervous System Neoplasms. J Mol Diagn. 2017:19(1):24-34.

6. Stupp R, Hegi ME, Mason WP, et al. Effects of radiotherapy with concomitant and adjuvant temozolomide versus radiotherapy alone on survival in glioblastoma in a randomised phase III study: 5-year analysis of the EORTC-NCIC trial. Lancet Oncol. 2009;10:459–66.

7. Mahat MYA, Ahamed NFA, Chandrasekaran S, et al. An improved method of transcutaneous cisterna magna puncture for cerebrospinal

fluid sampling in rats. J Neurosci Methods. 2012;211:272–9.

8. Scheinin I, Sie D, Bengtsson H, et al. DNA copy number analysis of fresh and formalin-fixed specimens by shallow whole-genome sequencing with identification and exclusion of problematic regions in the genome assembly. Genome Res. 2014;24(12):2022-32.

9. Noebauer-Huhmann IM, Szomolanyi P, Juras V, et al. Gadolinium-based magnetic resonance contrast agents at 7 Tesla: in vitro T1 relaxivities in human blood plasma. Invest Radiol. 2010;45(9):554-8.

10. Tofts PS, Brix G, Buckley DL, et al. Estimating kinetic parameters from dynamic contrast-enhanced T(1)-weighted MRI of a diffusable tracer: standardized quantities and symbols. J Magn Reson Imaging. 1999;10(3):223-32.

11. McGrath DM, Bradley DP, Tessier JL, et al. Comparison of model-based arterial input functions for dynamic contrast-enhanced MRI in tumor bearing rats. Magn Reson Med. 2009;61(5):1173-84.

12. Ju YS, Alexandrov LB, Gerstung M, et al. Origins and functional consequences of somatic mitochondrial DNA mutations in human cancer. eLife 2014. eLife.02935

13. Fliss MS, Usadel H, Caballero OL, et al. Facile detection of mitochondrial DNA mutations in tumors and bodily fluids. Science. 2000;287:2017–9.

14. Mair RJ, Wright A, Ros S, et al. Metabolic imaging of c-Myc expression in orthotopically implanted patient-derived xenograft models of glioblastoma. Cancer Res. 2018 Jul 27. Epub ahead of print.

15. Yung WK, Luna M, Borit A. Vimentin and glial fibrillary acidic protein in human brain tumors. J Neurooncol. 1985;3:35–8.

16. Lee J, Kotliarova S, Kotliarov Y, et al. Tumor stem cells derived from glioblastomas cultured in bFGF and EGF more closely mirror the phenotype and genotype of primary tumors than do serum-cultured cell lines. Cancer Cell. 2006;9:391–403.

17. Su Y-H, Wang M, Brenner DE, et al. Detection of Mutated K- rasDNA in Urine, Plasma, and Serum of Patients with Colorectal Carcinoma or Adenomatous Polyps. Ann N Y Acad Sci. 2008;1137:197–206.

18. Armstrong RC, Aja TJ, Hoang KD, et al. Activation of the CED3/ICE-related protease CPP32 in cerebellar granule neurons undergoing apoptosis but not necrosis. J Neurosci. 1997;17:553–62.

19. Jiang P, Chan CW, Chan KC,et al. Lengthening and shortening of plasma DNA in hepatocellular carcinoma patients. Proc Natl Acad Sci U S A. 2015;112(11):E1317-25.

20. Dubois LG, Campanati L, Righy C, et al. Gliomas and the vascular fragility of the blood brain barrier. Front Cell Neurosci. 2014;8:418.

21. De Mattos-Arruda L, Mayor R, Ng CKY, et al. Cerebrospinal fluid-derived circulating tumour DNA better represents the genomic alterations of brain tumours than plasma. Nat Commun. 2015;6:1–6.

22. Wang Y, Springer S, Zhang M, et al. Detection of tumor-derived DNA in cerebrospinal fluid of patients with primary tumors of the brain and spinal cord. Proc Natl Acad Sci USA. 2015;112:9704-9.

23. Lee HB, Blaufox MD. Blood volume in the rat. J Nucl Med. 1985;26(1):72-6.

24. Cosolo WC, Martinello P, Louis WJ, et al. Blood-brain barrier disruption using mannitol: time course and electron microscopy studies. Am J Physiol. 1989;256:R443–7.

25. Diehl F, Schmidt K, Choti MA, et al. Circulating mutant DNA to assess tumor dynamics. Nat Med. 2007;14:985–90.

26. Sage MR, Wilson AJ. The blood-brain barrier: an important concept in neuroimaging. AJNR Am J Neuroradiol. 1994;15:601–22.

27. Thierry AR, Mouliere F, Gongora C, et al. Origin and quantification of circulating DNA in mice with human colorectal cancer xenografts. Nucleic Acids Res. 2010;38:6159–75.

28. Rago C, Huso DL, Diehl F, et al. Serial Assessment of Human Tumor Burdens in Mice by the Analysis of Circulating DNA. Cancer Res. 2007;67:9364–70.

29. Pentsova EI, Shah RH, Tang J, et al. Evaluating Cancer of the Central Nervous System Through Next-Generation Sequencing of Cerebrospinal Fluid. J Clin Oncol. 2016;34:2404-15.

30. Hasbun R, Abrahams J, Jekel J, et al. Computed tomography of the head before lumbar puncture in adults with suspected meningitis. N Engl J Med. 2001;345:1727–33.

31. Engelborghs S, Niemantsverdriet E, Struyfs H, et al. Consensus guidelines for lumbar puncture in patients with neurological diseases. Alzheimers Dement (Amst). 2017;8:111–26.

32. Abdulla S, Saada J, Johnson G, et al. Tumour progression or pseudoprogression? A review of post-treatment radiological appearances of glioblastoma. Clin Radiol. 2015;70:1299–312.

33. Johnson BE, Mazor T, Hong C, et al. Mutational analysis reveals the origin and therapy-driven evolution of recurrent glioma. Science. 2014;343:189–93.

34. Kim J, Lee I-H, Cho HJ, et al. Spatiotemporal Evolution of the Primary Glioblastoma Genome. Cancer Cell. 2015;28:318–28.

35. Wang J, Cazzato E, Ladewig E, et al. Clonal evolution of glioblastoma under therapy. Nat Genet. 2016;48:768–76.

36. Mouliere F, Piskorz AM, Chandrananda D, et al. Selecting Short DNA Fragments In Plasma Improves Detection Of Circulating Tumour DNA. bioRxiv. 2017; https://doi.org/10.1101/134437.

37. Jahr S, Hentze H, Englisch S, et al. DNA fragments in the blood plasma of cancer patients: quantitations and evidence for their origin from apoptotic and necrotic cells. Cancer Res. 2001;61:1659–65.

38. Lo YM, Chan KC, Sun H, et al. Maternal plasma DNA sequencing reveals the genome-wide genetic and mutational profile of the fetus. Sci Transl Med. 2010;2(61):61ra91.

39. Mouliere F, Robert B, Arnau Peyrotte E, et al. High fragmentation characterizes tumour-derived circulating DNA. PLoS One. 2011;6(9):e23418.

40. Underhill HR, Kitzman JO, Hellwig S, et al. Fragment Length of Circulating Tumor DNA. PLoS Genet. 2016;12(7):e1006162.

41. Snyder MW, Kircher M, Hill AJ, Cell-free DNA Comprises an In Vivo Nucleosome Footprint that Informs Its Tissues-Of-Origin. Cell. 2016;164(12):57-68.

42. Sun K, Jiang P, Chan KC, et al. Plasma DNA tissue mapping by genome wide methylation sequencing for noninvasive prenatal, cancer, and transplantation assessments. Proc Natl Acad Sci U S A. 2015;112(40):E5503-12.

43. Sun K, Jiang P, Wong AIC, et al. Sizetagged preferred ends in maternal plasma DNA shed light on the production mechanism and show utility in noninvasive prenatal testing. Proc Natl Acad Sci U S A. 2018;115(22):E5106-E5114.

44. Gray LH, Conger AD, Ebert M, et al. The concentration of oxygen dissolved in tissues at the time of irradiation as a factor in radiotherapy. Br J Radiol. 1953;26:638–48.

45. Yeung K, Dickinson A, Donoghue JF, et al. The identification of mitochondrial DNA variants in glioblastoma multiforme. Acta Neuropathol Commun. 2014;2:1.

46. Yuan Y, Ju YS, Kim Y, et al. Comprehensive Molecular Characterization of Mitochondrial Genomes in Human Cancers. 2017;biorxiv: https://doi.org/10.1101/161356

47. Grandhi S, Bosworth C, Maddox W, et al. Heteroplasmic shifts in tumor mitochondrial genomes reveal tissue-specific signals of relaxed and positive selection. Hum Mol Genet. 2017;26(15):2912-2922.

48. Newman AM, Lovejoy AF, Klass DM, et al. Integrated digital error suppression for improved detection of circulating tumor DNA. Nature Biotechnology. 2016;34:547–55.

49. Reznik E, Miller ML, Senbabaoglu Y, et al. Mitochondrial DNA copy number variation across human cancers. eLife. 2016; eLife.10769.

50. Guerra F, Perrone AM, Kurelac I, et al. Mitochondrial DNA mutation in serous ovarian cancer: implications for mitochondria-coded genes in chemoresistance. J Clin Oncol. 2012;30:e373–8.

Figure legends

Figure 1 Validation of the specificity and sensitivity of the ctDNA and tmtDNA dPCR assays. a) dPCR assays designed to detect ctDNA, tmtDNA and non-tumor cell-free (nt cfDNA) were tested with human and rat plasma DNA. Samples were tested in quadruplicate for each assay. ND indicates non-detectable. b) Dilution series of human (tumor) DNA in rat (non-tumor) DNA, which was used to evaluate the sensitivity of tmtDNA detection in comparison to detection of ctDNA. tmtDNA was detected at 100x greater dilution than ctDNA. Each sample was measured in duplicate.

Figure 2 tmtDNA was detected more frequently in plasma than ctDNA. a) Detection rates for plasma circulating cell-free tumor DNA (ctDNA), tumor mitochondrial DNA (tmtDNA) and non-tumor (rat host) cell-free DNA (nt cfDNA) in 64 animals implanted orthoptopically with cells derived from tumors from 6 different patients. b) Concentration (copies/mL) of circulating nucleic acids in the samples where these were detected. ctDNA (c) and tmtDNA concentrations (d) in CSF, plasma and urine from the tumor-bearing animals. In the ratios shown below the plots in (c) and (d) the numerator represents the number of samples containing the indicated DNA and the denominator the number of samples.

Figure 3 Factors affecting the levels of ctDNA and tmtDNA in the plasma of treatment-naïve tumor-bearing rats. Principal component analysis of variables associated with tumor histology and circulating nucleic acids in the plasma of rats with GB4 tumors (n=36). The vectors represent ctDNA, tmtDNA and non-tumor cfDNA concentrations, tumor volume, tumor proliferation (Ki67), hypoxia (CAIX), necrosis (TUNEL) and apoptosis (CC3). PC1 (44.9%) and PC2 (25.1%) indicate the % variance accounted for by the two principal components.

Figure 4 Factors affecting the levels of ctDNA and tmtDNA in the plasma of tumor-bearing rats following concomitant Temozolomide and radiotherapy treatment. a) Correlation between tumor volume and the concentrations of ctDNA, tmtDNA and nt cfDNA in the plasma of animals with GB4 tumors (n=36) determined by dPCR. b) ctDNA and tmtDNA levels in a subset of 7 rats with GB4 tumors that received 15 Gy with concurrent temozolomide, and 5 rats with untreated GB4 tumors that were analyzed as controls (no_RT). Panels c and d show levels of cell death in the tumors of these GB4 models determined by TUNEL and CC3 staining.

Figure 5 The fragmentation patterns of plasma DNA in tumor-bearing animals. a) Sequencing reads were obtained by paired-end shallow WGS of plasma DNA and aligned to the human (tumor) and rat (host) genomes. b) Copy number profiles obtained from sWGS of DNA from tumor tissue, CSF and plasma from the GB4 model (n=3), separated into reads that aligned with the human and rat genome. c) Size distribution of DNA fragments of nuclear origin from a plasma sample from the GB6 model. ctDNA fragments originating from tumor cells, aligned to the human genome, are shown in red, whereas nt cfDNA fragments from host cells, aligned to the rat genome, are shown in blue. A vertical line (at 167 bp) indicates fragment sizes associated with nt cfDNA of apoptotic origin. d) Size distribution of the DNA fragments of nuclear origin from a plasma sample from a GB4 tumor-bearing animal. e) Size distribution of the DNA fragments of nuclear origin from a CSF sample from a GB4 tumor-bearing animal. f) Size distribution of mitochondrial DNA fragments from a plasma sample: tmtDNA originating from tumor cells,

aligned to the human mitochondrial genome, are shown in purple, and non-tumor mitochondrial DNA, aligned to the rat genome, are shown in green.

Figure 6 The integrity of the blood brain barrier has little effect on ctDNA and tmtDNA levels in plasma. a) Pairwise comparison of tmtDNA in plasma and CSF collected at the same time from 10 GB4 tumor-bearing animals and two U87 tumor-bearing animals. Concentrations determined in the CSF are plotted relative to the concentration detected in plasma samples. b) Concentrations of ctDNA and tmtDNA, normalized to tumor volume, in the plasma of GB4 tumor-bearing rats, where the tumors were implanted orthotopically (n=5), with or without disruption of the BBB by mannitol injection (n=6), or where the tumors were implanted subcutaneously (n=5). There were no significant differences in the concentrations of ctDNA or tmtDNA between these groups (ANOVA $p=0.57$ and individual paired t-tests ($p>0.2$); n=16). c) Microvessel density in each tumor model (n=3 per cohort), as analyzed by in situ hybridization with a CD31 mRNA probe. d) Plasma ctDNA and tmtDNA concentrations in animal models with tumors that showed signal enhancement (n=22; GB1,3,4), and those that did not enhance (n=18; GB1,2,3,4), in T_1-weighted MR images following administration of a gadolinium-based contrast agent. There was no significant difference between the groups ($p=0.26$). Additional points represent outliers.

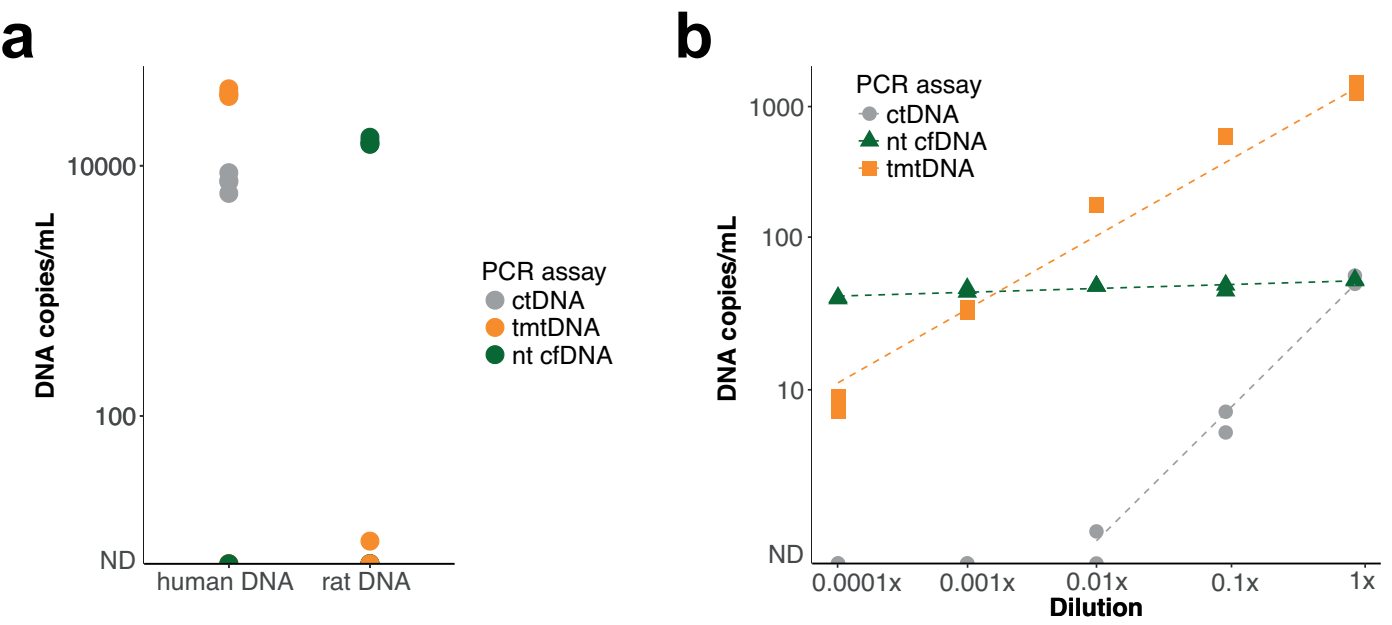

Figure 1

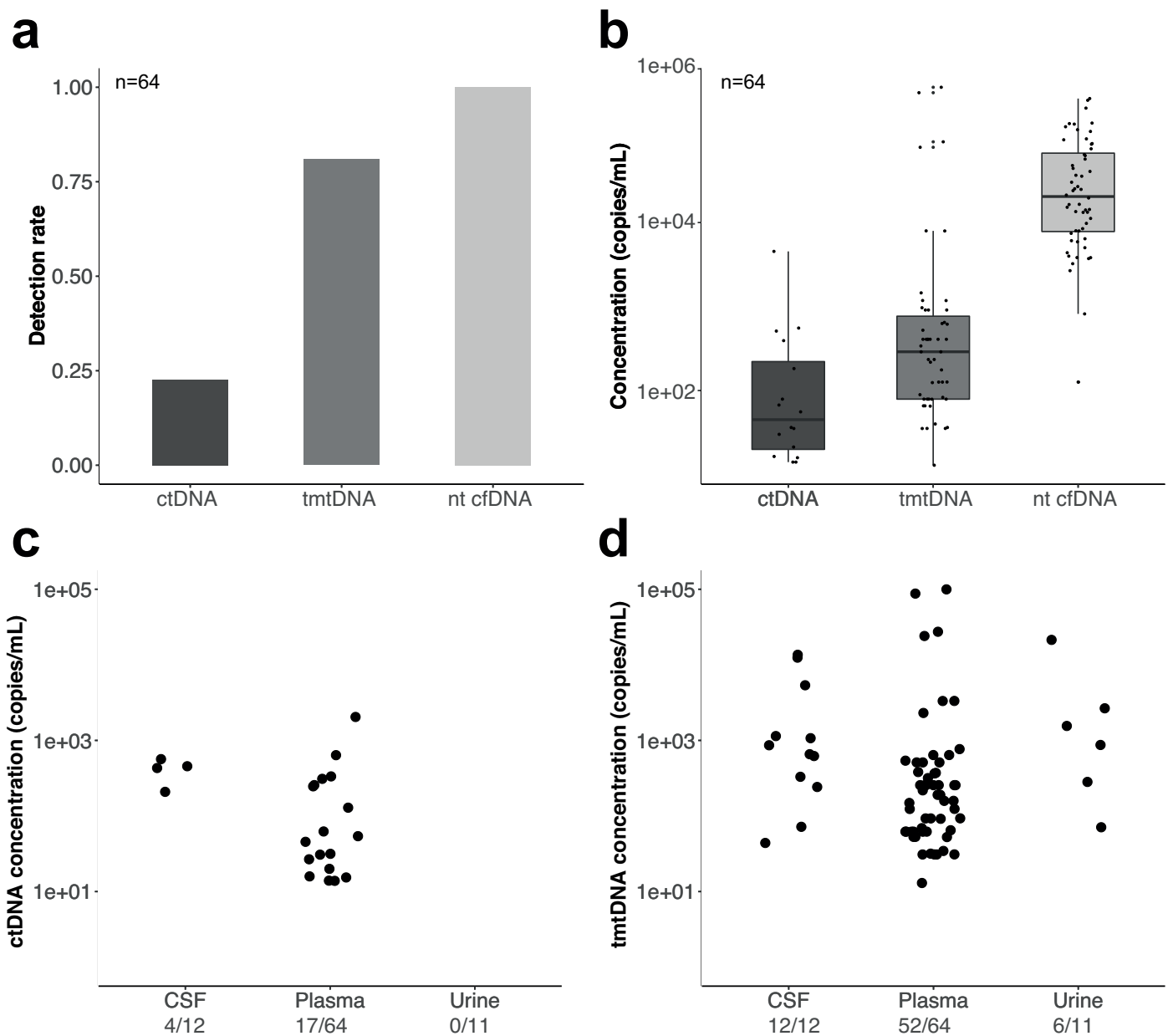

Figure 2

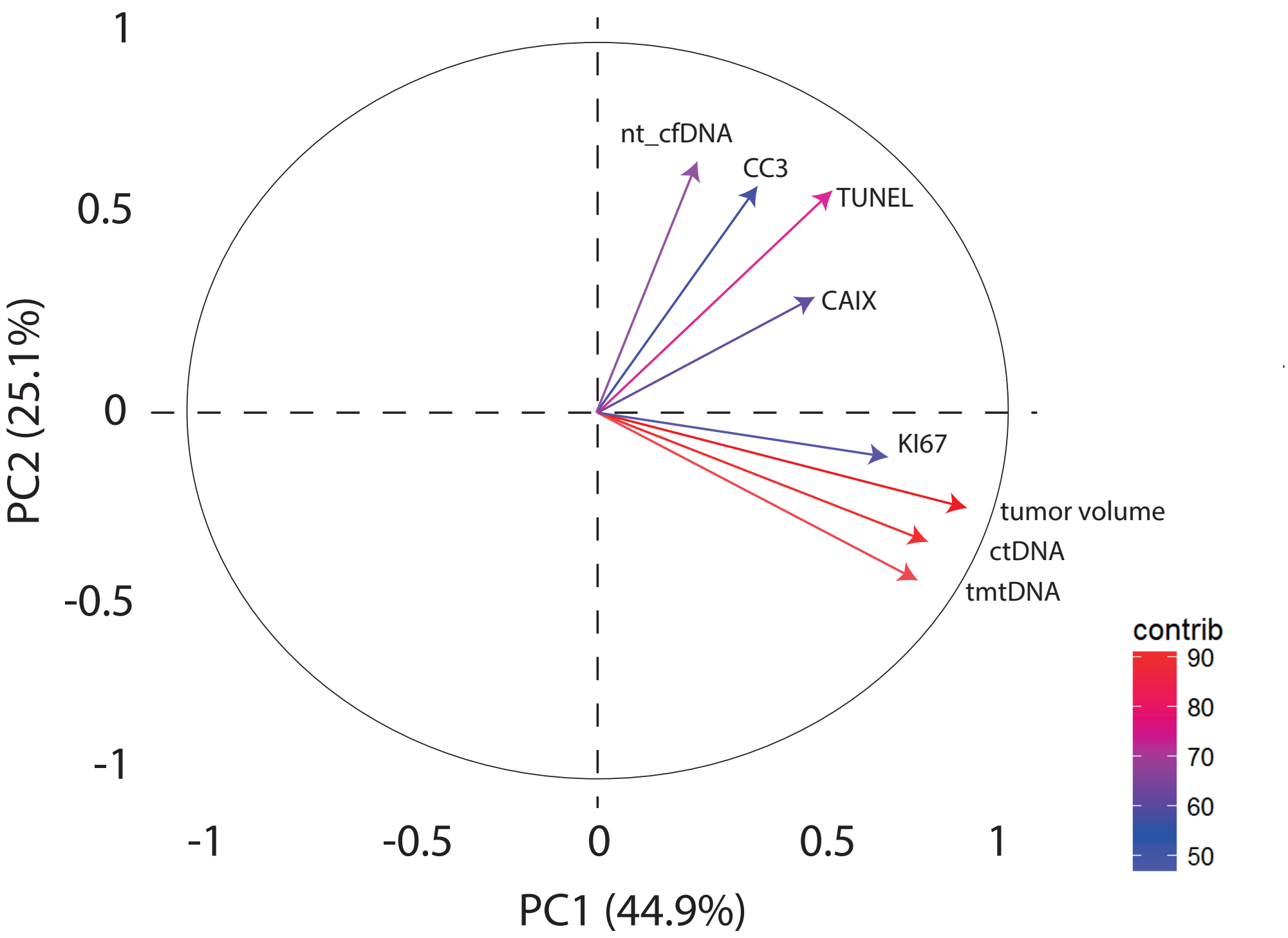

Figure 3

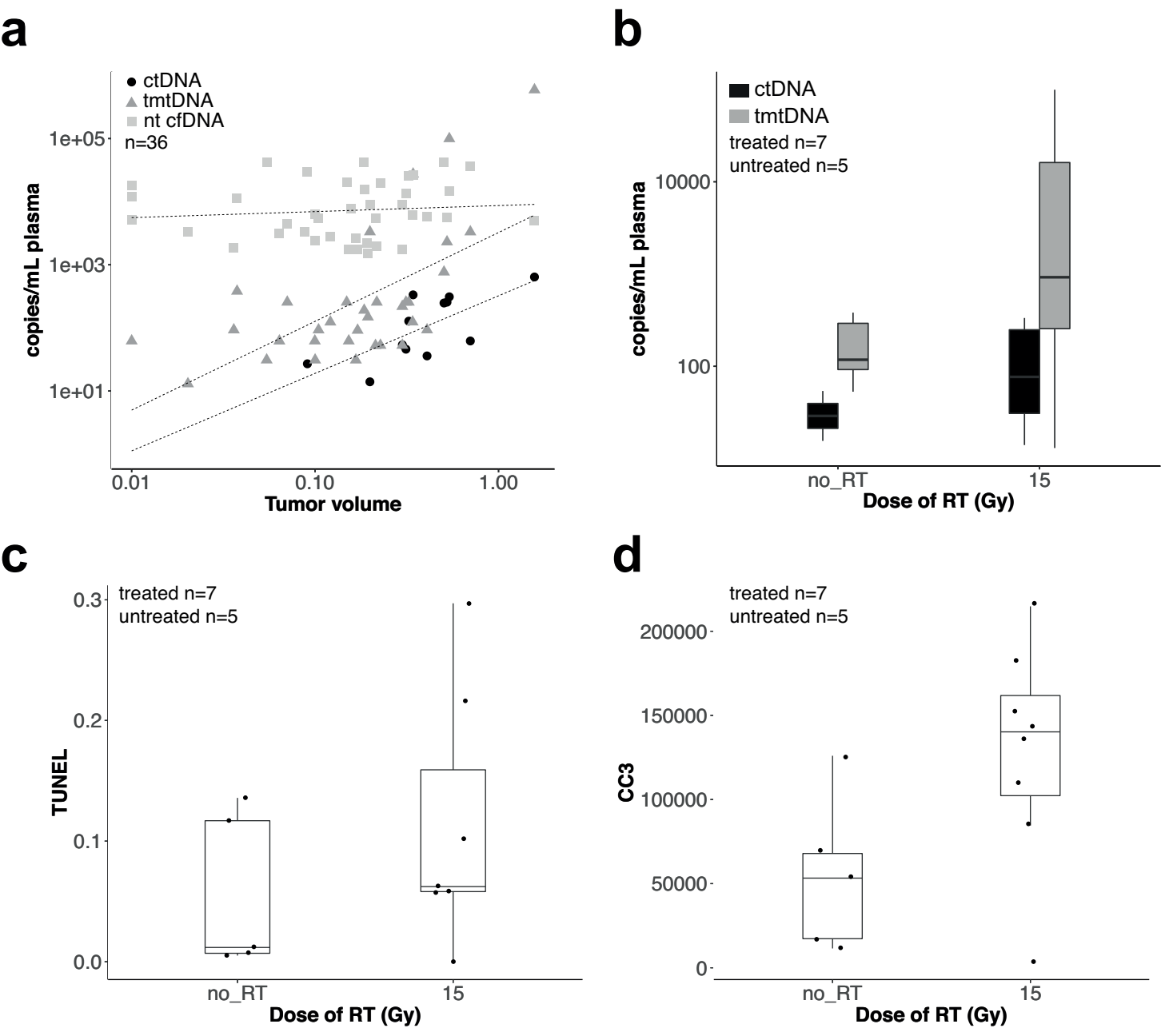

Figure 4

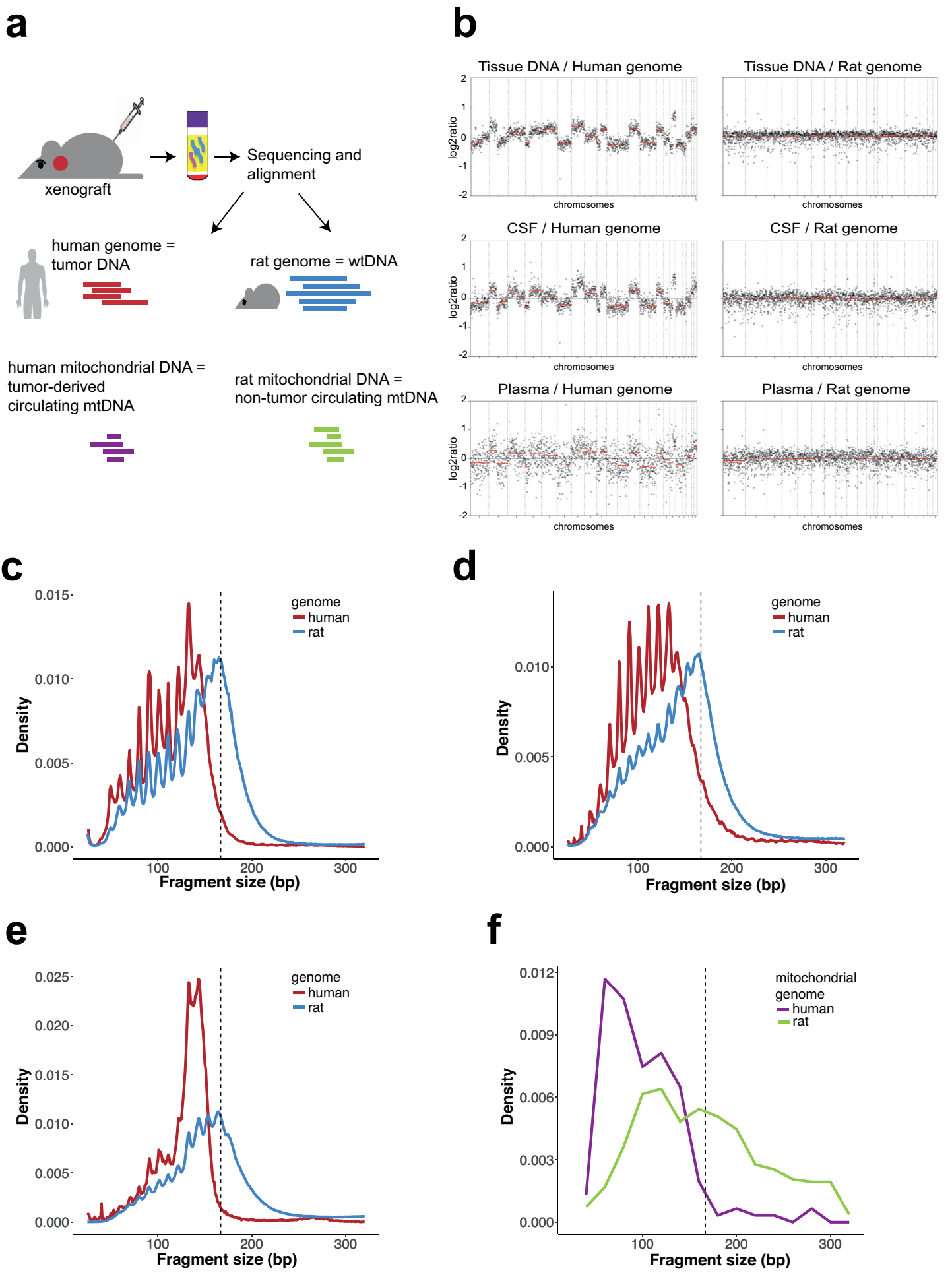

Figure 5

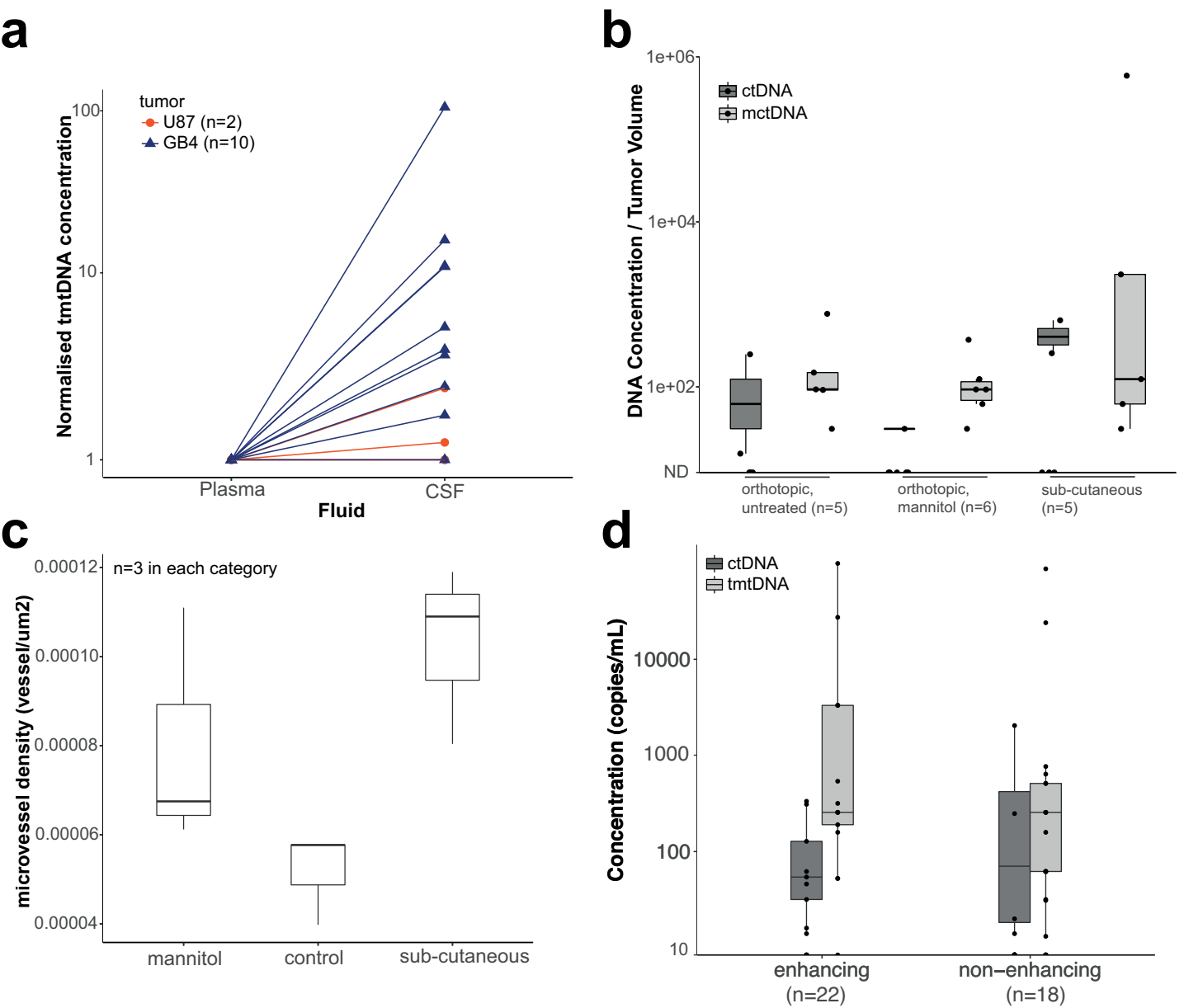

Figure 6

AACR American Association for Cancer Research

Cancer Research

The Journal of Cancer Research (1916–1930) | The American Journal of Cancer (1931–1940)

Measurement of plasma cell-free mitochondrial tumor DNA improves detection of glioblastoma in patient-derived orthotopic xenograft models.

Richard Mair, Florent Mouliere, Christopher G Smith, et al.

Cancer Res Published OnlineFirst November 2, 2018.